I&EC research
Industrial & Engineering Chemistry Research
pubs.acs.org/IECR
Article

Investigation on Designing Meltblown Fibers for the Filtering Layer of a Mask by Cross-Scale Simulations

Jie Shi, Yuanzuo Zou, Jie-Xin Wang, Xiao-Fei Zeng, Guang-Wen Chu, Bao-Chang Sun,* Dan Wang,* and Jian-Feng Chen

Cite This: *Ind. Eng. Chem. Res.* 2021, 60, 1962−1971
Read Online
ACCESS | Metrics & More | Article Recommendations

ABSTRACT: As an important personal protective item against the COVID-19 pandemic, masks have recently attracted much attention in both academic and industrial contexts. We established a modified numerical model for investigating the dominant factors on the performance of masks, including the thickness and fill rate of melt-blown fibers for a filtering layer, as well as the diameters and surface charge density of the fibers. It is found that increasing the surface charge of melt-blown fibers can improve the filtration efficiency of the melt-blown layer with a low respiratory pressure drop. The relationship between the filtered particle diameter and filtration efficiency of respirators is also investigated, which demonstrated that particles with a diameter of 0.1−0.2 μm are the most difficult to filter out. Combined with molecular dynamics simulations and experimental verifications, the effect of hydrophobicity on the droplet adhesion and the water blocking performance was revealed. The knowledge obtained in this work provides reference for the design of high-performance masks.

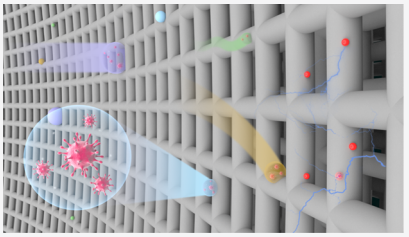

1. INTRODUCTION

Respirators, which are commonly known as masks, are essential necessities to fight against the pandemic of the worldwide coronavirus disease 2019 (COVID-19).[1] Since the COVID-19 pandemic in 2020, people are recommended globally to wear masks in public places such as supermarkets, shopping malls, subways, and so on.[2] To date, commercialized masks are usually made of three layers of nonwoven polypropylene fabric, including the inner layer, filter layer, and the outer layer. Typically, the inner layer of a respirator is designed to absorb the moisture released from wearers. The outer layer mainly works as the structural support and also can block large particles and liquid droplets. The filter layer is the most crucial; it is usually made of charged melt-blown polypropylene microfibers or polymeric nanofibers, serving as the barrier against fine particulate matter, which may contain germs.[3] Meanwhile, the limited productivity and scarce resources cannot meet the ever-increasing demand of respirators; some government institutions and academic communities recommended using cloth respirators when at low infection risk and when there is lack of new melt-blown fiber respirators.[4]

Besides national or industrial standard requirements on respirators properties, some other requirements are equally essential, such as high bacterial filtration efficiency (BFE) and/or particle filtration efficiency (PFE) to block microorganisms, droplets, other particles, as well as low-enough air resistance to ensure the wearing comfort of users. Increasing the thickness and fill rate of the respirator can directly increase the filtration efficiency and also increase the respiratory resistance, that is, the increase in gas diffusion resistance caused by the increase in particle filtration efficiency for respirators. Therefore, introducing static charge on the surfaces of the respirator fibers to adsorb particles can partially solve the contradiction. The other option to solve this contradiction is represented by the application of nanofiber technology. By using nanofibers with an ultrasmall diameter, high surface-area-to-volume ratio and high porosity are achieved; thus, the filtration efficiency could be significantly enhanced, while the filtration pressure drop may also decrease, compared to microfiber respirators.[5] Many researchers have investigated influences of structural parameters (i.e., fiber diameter, thickness, porosity, fill rate, and charge density) on the filtration process of different filtered objects (i.e., oil particulates, nonoil particulates, germs, virus, and volatile organic compounds).[6−8] Particularly, because of the global shortage of respirators supply and the environmental problems caused by difficulty in recycling, Tudu et al.[9] have developed a self-powered triboelectric respirator for long-time effective use on the basis of the general recognition that electrostatic charge can improve the performance of respirators. For the same purpose, worldwide researchers give efforts

Received: December 20, 2020
Revised: January 8, 2021
Accepted: January 11, 2021
Published: January 20, 2021

https://dx.doi.org/10.1021/acs.iecr.0c06232
Ind. Eng. Chem. Res. 2021, 60, 1962−1971

on the recycling and reuse of respirators and gave better regeneration plans.[3,10,11] On this basis, it can be anticipated that the theoretical modeling of the structure−effect relationship of the respirator will help to design and use the melt-blown cloth more efficiently, thus to greatly reduce the supply pressure and performance concerns. From a dialectical perspective, the performance of a respirator is controlled by two dominant mechanisms: particle filtration and gas diffusion. Therefore, the cognation of how the various factors work in the micro−nano multiscale is very useful, especially for the design of the filtration material and respirator structure.

In this work, we investigate the complexity of designing a respirator by a modified numerical model for calculation of melt-blown intermediate layer pressure drop and filtration efficiency. The effects of thickness, fill rate, surface charge density, and fiber diameter on the performance of respirators are studied. Moreover, through classical molecular dynamics (MD) simulations, the influence of the surface affinity of the melt-blown fiber on the filtration performance and the abilities of different diameters fibers to break particulates is demonstrated.

2. THEORY AND MODEL

2.1. Model Assumptions. A model suitable for the filtration performance of the melt-blown layer of the respirator is established. The basic assumptions are as follows:

- The fiber filter material can be regarded as a stack of multiple fiber layers perpendicular to the airflow direction, and it is assumed that the fibers in the fiber medium are evenly distributed and the fiber diameter is uniform (equaling to the average fiber diameter).
- Various influence factors act independently on particulate filtration.
- The hydrophilicity of the melt-blownfiber surface and whether the particulate is oily or water-based are ignored (Except for MD simulations).
- Particles deposited in the melt-blown layer have no effect on the filtration performance. In other words, the model in this paper is only suitable for the prediction of the initial filtration performance of clean melt-blown nonwoven fabrics.
- Reynolds number of airflow through the melt-blown layer has no effect on the filtration performance model. The Reynolds number is defined as $Re = (\rho v d_f)/\mu$, where v is the face velocity (~0.18 m/s when flux is 85 L/min, and the radius of flow surface is 5 cm), d_f is the fiber diameter (3 μm here), and μ is the dynamic viscosity of air (15.7 μPa·s here). It much smaller than 1, indicating that the flows are in the Stokes flow regime, which is similar to previous research studies.[12,13]

2.2. Mechanical Filtration Efficiency. The relationship between the total mechanical filtration efficiency and the particle mechanical penetration rate of the melt-blown layer can be calculated by eq 1

$$E_m = 1 - P_m \tag{1}$$

where P_m is the particle mechanical penetration rate of the filter. In the current research studies of air filtration theory, the integral filtration material mechanical filtration theory developed from the single-fiber filtration model proposed by Lee and Liu[14] has gained some approvals.[15,16] *Based on the assumption of uniform fiber media,* P_m should be related to the fiber diameter, fiber fill rate (volume fraction), filter thickness, and the contribution of single fiber capture efficiency. P_m can be expressed by eq 2

$$P_m = 1 - e^{(-4\alpha E_T Z/\pi d_f(1-\alpha))} \tag{2}$$

where d_f is the fiber diameter, α and Z are the fiber volume fraction and thickness of filter material, respectively. E_T is the total mechanical filtration efficiency of a single fiber and can be described as

$$E_T = E_D + E_C + E_{DC} + E_I + E_G \tag{3}$$

E_D, E_C, E_I, and E_G correspond to the capture efficiency because of diffusion, collision interception, inertia, and gravity, respectively. E_{DC} represents the enhanced capture efficiency due to particle diffusion as Hinds mentioned.[17]

2.3. Components of Single Fiber Filtration Efficiency. The Peclet number, *Pe*, as the ratio of convection strength and diffusion strength, has always been an important object to study the single fiber filtration efficiency caused by diffusion.[18] The calculation methods of E_D are given in the form of eq 4. Empirically, for submicron particles, E_D accounts for more than half of the total filtration efficiency of a single fiber.

$$E_D = APe^m \tag{4}$$

where A and m are two constants (as the report of Wang et al.[12]; A = 0.81 to 0.87 and m = −0.46 to −0.41), and Pe is given as

$$Pe = \frac{d_f v}{kTB} \tag{5}$$

where v, k, and T account for gas velocity, Boltzmann constant, and temperature (300 K here), respectively. B is the mechanical mobility of the particles in air, and it should be related to gas dynamic viscosity, particle size, and particle−gas interaction

$$B = \frac{C_c}{3\pi\mu d_p} \tag{6}$$

where μ is the gas dynamic viscosity (15.7 μPa·s here), d_p is the characteristic size of particles (the spherical particle model is used here, so it is the particle diameter), and C_c is the Cunningham slip correction factor related to particle−gas interaction, and its expression is

$$C_c = 1 + \frac{\lambda}{d_p}[2.34 + 1.05\, e^{(-0.39 d_p/\lambda)}] \tag{7}$$

where λ is the mean free path of gas molecules.

As for the capture efficiency E_C caused by collision interception, intuitively, it should be related to the fiber fill rate, particle, and fiber size. Based on the Kuwabara flow field model,[19,20] E_C can be written as

$$E_C = \frac{1+R}{2Ku}\left[2\ln(1+R) + \left(\frac{1}{1+R}\right)^2\left(1-\frac{\alpha}{2}\right) - \frac{\alpha}{2}(1+R)^2 + \alpha - 1\right] \tag{8}$$

where R is the ratio of particle diameter (d_p) to fiber diameter (d_f); Ku is the Kuwabara hydrodynamic factor and defined as

https://dx.doi.org/10.1021/acs.iecr.0c06232
Ind. Eng. Chem. Res. 2021, 60, 1962−1971

$$\mathrm{Ku} = -\frac{\ln \alpha}{2} - \frac{\alpha^2}{4} + \alpha - \frac{3}{4} \tag{9}$$

As Hinds reported,[17] the enhanced capture efficiency due to particle diffusion (E_{DC}) should be related to the spatial characteristics of the flow field and the characteristics of the fluid, so it can be expressed as

$$E_{DC} = \frac{1.24R^{2/3}}{(\mathrm{Ku} \times Pe)^{0.5}} \tag{10}$$

E_I characterizes the enhancement of fiber interception particles by the degree of particle inertial motion with fluid, and it should be related to the Stokes number, which describes the degree of suspended particles affected by the inertia of the gas. As reported by Wang et al.,[13] the spatial characteristics of the flow field (such as fiber fill rate and sizes of particle and fiber) can also affect E_I

$$E_I = \frac{1}{(2\mathrm{Ku})^2}[(29.6 - 28\alpha^{0.62})R^2 - 27.5R^{2.8}]\mathrm{Stk} \tag{11}$$

where Stk is the Stokes number; the smaller the particles, the easier it is to follow the movement of the fluid.

$$\mathrm{Stk} = \frac{\rho_p {d_p}^2 C_c v}{18\mu d_f} \tag{12}$$

where ρ_p is the particle density (2.165×10^3 kg/m^3 for the NaCl particle here). As for the enhancement of the trapping efficiency due to the gravity effect (E_G), it can be ignored for filtering submicron particles. So far as we know, the calculation of mechanical filtration efficiency has been completed.

2.4. Electrostatic Filtration Efficiency. For the calculation of the filtration efficiency of the electret filter material (E_e), this article follows the formula reported by Yu and Zhao[21]

$$E_e = 1 - P_e = 1 - P_m\tau \tag{13}$$

where P_e is the particle penetration rate of the electret filter material; τ is the electrostatic enhancement factor that should be related to particle size, surface charge density, and gas velocity

$$\tau = \left(\frac{d_p}{d_c}\right)^{-K\sigma[-\ln(v)+1]} \tag{14}$$

where d_c is the critical particle size of electrostatic effect (as Chang et al. reported;[22] when the particle diameter is less than 20 nm, the presence of static electricity does not improve the filtration efficiency, so d_c = 20 nm); K is a constant (2664.2) fitted from experimental data.[21]

2.5. Pressure Drop. The pressure drop should be related to the gas dynamic viscosity, fiber fill rate, filter thickness, gas velocity, and fiber diameter. According to the form of Darcy's law, it can be expressed as

$$\Delta P = C_d \frac{4\mu\alpha v Z}{\pi {d_f}^2} \tag{15}$$

in which C_d is the drag coefficient. After comparing with the experimental data of respirators' pressure drop, it is found that the pressure drops of the filter obtained by the above C_d calculation methods are too large; then, we choose Hinds's method[17] and modify it as

$$C_d = 4\pi\alpha^{0.5}(1 + 56\alpha^3) \tag{16}$$

The polymer density (fiber density ρ_f) is set as 900 kg/m^3. For the calculation of the areal density (D_{areal}) of the respirator, follow the formula

$$D_{areal} = \alpha\rho_f Z \tag{17}$$

2.6. MD Simulation Models and Methods. MD simulations are performed on a large-scale atomic/molecular massively parallel simulator (LAMMPS).[23] Both the X and Y spatial dimensions of the simulated box use periodic boundary conditions, and the Z dimension (perpendicular to the surface or parallel to the droplet movement) uses nonperiodic elastic reflection boundary conditions. As shown in Table 1, the SPC/E H_2O model is adopted, and the long-range charge interaction between H_2O molecules is calculated by the PPPM method with a cutoff distance of 12 Å, which means that interactions outside the distance are computed in reciprocal space. The equations of motion are integrated with the velocity Verlet algorithm with a time step of 1 fs. The temperatures of all MD simulations are set to 300 K, controlled with the Nosé-Hoover thermostat of a relaxation time of 0.10 ps.

Table 1. LJ Potential Parameters and Atomic Charges for MD Simulation Systems

	LJ potential parameters		atomic charges
atom type	σ (kcal/mol)	r (Å)	e
O of H_2O	0.1553000	3.166	−0.8476
H of H_2O	0	0	0.4238
C of 134° surface	0.0055688	3.400	0.0000
C of 116° surface	0.0155688	3.400	0.0000
C of 91° surface	0.0555688	3.400	0.0000
C of 66° surface	0.1055688	3.400	0.0000
C of 34° surface	0.1555688	3.400	0.0000
C of 0° surface	0.2055688	3.400	0.0000

2.6.1. MD Simulation 1. Fixed graphene surfaces with different Lennard-Jones (LJ) potential parameters in Table 1 are used to study the droplet adhesion performance of different affinity surfaces. The LJ potential function is given by[24]

$$U_{LJ}(r) = 4\varepsilon\left[\left(\frac{\sigma}{r}\right)^{12} - \left(\frac{\sigma}{r}\right)^{6}\right] \tag{18}$$

The 20 × 35 graphene surface and droplet (1000 H_2O molecules) model are prerelaxed for 2 ns, and the sampling of the contact angle is time-averaged within the subsequent 1 ns. The calculation of the contact angle follows the volume-contact area method,[25] which is suitable for the calculation of the contact angle of droplets of any shape than the fitted edge method. Subsequently, a variable force is applied to the center of the droplet mass and makes it moves upward in the Z direction at a speed of 5 Å/ns, and the force of the process is integrated to obtain the potential of mean force (PMF).

2.6.2. MD Simulation 2. In the study of the water blocking performance of different affinity polymer fiber networks (melt-blown cloth microstructures), a (40, 40) single-wall carbon nanotube (SWCNT) (diameter ∼54.24 Å, length ∼30 Å) embedded vertically between two layers of graphene is chosen to model the pores in the melt-blown layer. The simulation box is a cube of ∼150 Å, filled with 29,988 H_2O molecules above the pore, and a monoatomic hard wall composed of

https://dx.doi.org/10.1021/acs.iecr.0c06232
Ind. Eng. Chem. Res. 2021, 60, 1962−1971

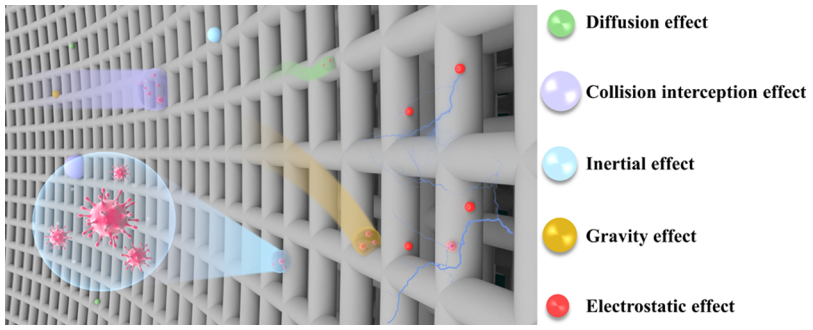

Figure 1. Filtration mechanism model of the melt-blown layer in respirators.

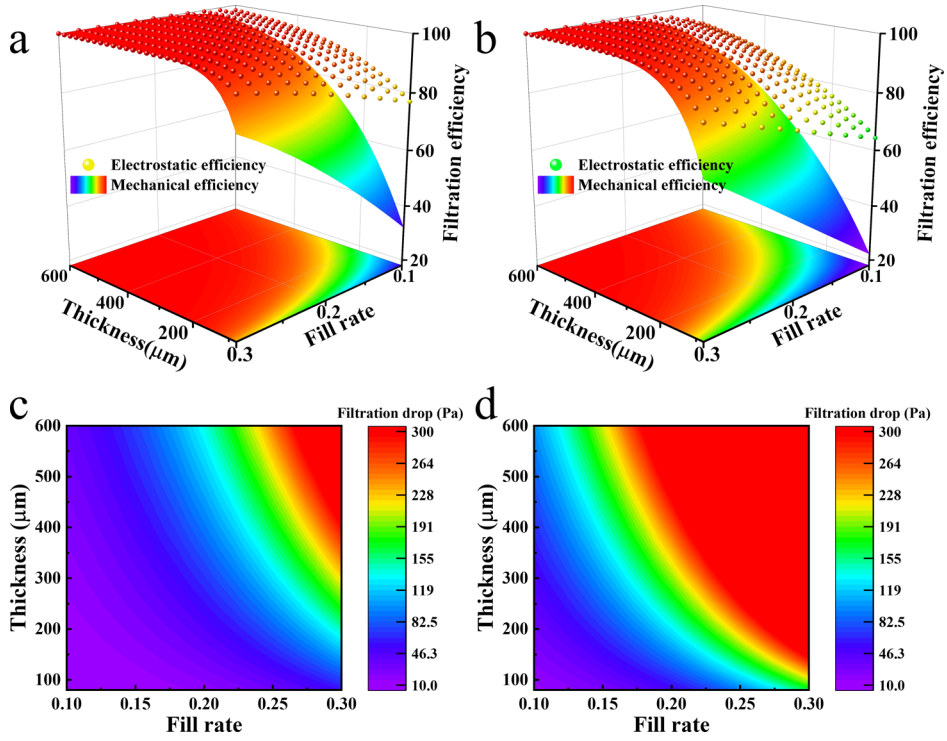

Figure 2. Filtration performance of melt-blown layers with different thicknesses and fiber fill rates at 30 L/min (a,c) and 85 L/min (b,d). The preconditions of the data above are fiber diameter, 3 μm; imposed surface charge density of fibers, 67 $\mu C/m^2$; filtering particles' diameter, 100 nm.

2500 C atoms is set to provide the driving force (differential pressure) required for water to pass through the pore. The LJ potential parameters of the C atoms corresponding to the surface with a contact angle of 0° and a contact angle of 134° used in simulation 1 are used for the simulations of hydrophilic and hydrophobic channels, respectively. The entire system first uses the setting of the virtual wall to close the SWCNT pore, then prerelaxes for 0.5 ns until the water layer is adsorbed to the upper graphene surface, and reaches the periodic boundary in the *xy* direction. After prerelaxation, the pore is opened to let the water flow through.

2.6.3. MD Simulation 3. For the characteristics of a simple structure and easy to adjust radius, the SWCNT is a good model for studying different fiber diameters. Furthermore, we have used the graphene model to explore the influence of hydrophilicity and hydrophobicity in MD simulation 1; therefore, it is not necessary to consider the surface affinity when choosing a SWCNT to study the influence of fiber diameters. In the simulations of droplet impact on fibers, to compare the performances of fibers with different diameters intuitively instead of caring about the material (in fact, the material part has also been explored a little by the change of surface hydrophilicity and hydrophobicity), (5, 5) SWCNT (diameter 6.78 Å) and (20, 20) SWCNT (diameter 27.12 Å) are used as fiber models with different diameters for convenience. The LJ potential parameters of SWCNT are the same as C atoms in the 134° surface in Table 1. The Z direction of the simulation box is set as 300 Å to sufficiently reproduce the droplet shape before and after impact; the SWCNT length is 167.25 Å in the periodic direction, and the last dimension is set as 160 Å to prevent the periodic interaction of the droplet from affecting its morphology. The initial droplets (include 1000 H_2O molecules) are tethered at a distance of 110 Å from the SWCNT and relaxed for 1 ns under the regular ensemble of 300 K. Subsequently, the droplet is given a velocity parallel to the *Z* direction, and a 0.1 ns impact simulation is performed under a microregular ensemble.

3. RESULTS AND DISCUSSION

The mechanism of intercepting particulates in the middle melt-blown layer is shown in Figure 1. The diffusion effect refers to

https://dx.doi.org/10.1021/acs.iecr.0c06232
Ind. Eng. Chem. Res. 2021, 60, 1962−1971

the influence of the thermal motion of air molecules on small particulates, which is caused by Brownian motion and can make them away from the streamline and hit the filter fiber. The collision interception effect means that the distance between the fiber and the streamline where the particle is located is less than its radius particle diameter, causing it to collide with the fiber, as the purple particles. The inertial effect means that large particles sometimes move away from the streamline because of inertia, causing them to eventually collide with the fiber. In addition, large particles are also vulnerable to gravity and deviate from the orbit, causing them to be intercepted, which is the gravity effect. The electrostatic effect means that the particulates in the airflow will be charged with static electricity because of motion friction or polarized by electric field induction, so that when it moves to the vicinity of the charged fiber, it is easily adsorbed and intercepted by electrostatic attraction.

In the production and use of respirators, the main factors that affect the filtration performance are the thickness, the fiber fill rate, the fiber diameter, the charge amount (electrostatic potential) of the middle melt-blown layer, and the size of the particles. The thickness of the melt-blown layer and the fill rate together determine the areal density (gram weight). According to the Chinese industrial standard YY 0469-2011 of medical surgical masks, a gas flow rate of (30 ± 2) L·min^{-1} was required for testing the PFE. According to the Chinese national standard GB 2626-2019 for KN95-grade masks, the gas flow rate should be (85 ± 2) L·min^{-1} during testing of PFE for nonoily particles. Therefore, the gas fluxes of 30 and 85 L/min and a cross-sectional area of 100 cm^2 are determined for simulations. As shown in Figure 2a,b, the effects of the melt-blown layer thickness and fiber fill rate on its filtration efficiency are investigated. As the fill rate and thickness increase, the filtration efficiency of the filter layer increases, and the changing trend of filtration efficiency is more obvious at a low thickness (<200 μm) and low fill rate (<20%). In addition, comparing the difference between electrostatic efficiency and mechanical efficiency, it is found that static electricity improves filtration efficiency more obviously at low mechanical efficiency, which also means that in respirators with sufficiently high mechanical efficiency, the electret process hardly improves the performance of the melt-blown layer. Figure 2c,d shows that as the thickness and fill rate increase, the filtration pressure drop continues to increase. It is generally believed that at a flux of 85 L/min, if the pressure drop of the respirator is higher than around 300 Pa and the total filtration efficiency is less than 95%, then it will be unacceptable and seriously affect the safety of users.

In addition, the influence of the surface charge density of fibers, which is easy to control in the production process and changes during use, on the filtration efficiency has been investigated. In the three typical respirator cases, as the surface charge density increases, the increase of the filtration efficiency becomes more and more gentle. It seems like that a 65 μC/m^2 surface charge density can achieve a good-enough enhancement of filtration efficiency from Figure 3 and continuing to increase the surface charge density may cost a lot. The two melt-blown layers (400−0.20 and 600−0.16) have reached more than 95% of the filtration efficiency in the absence of static electricity and increasing the surface charge density can only enhance its efficiency by around 2−4%.

The data plotted in Figures 4 and 5 are the filtration performances as the fiber diameters and fill rates changing at

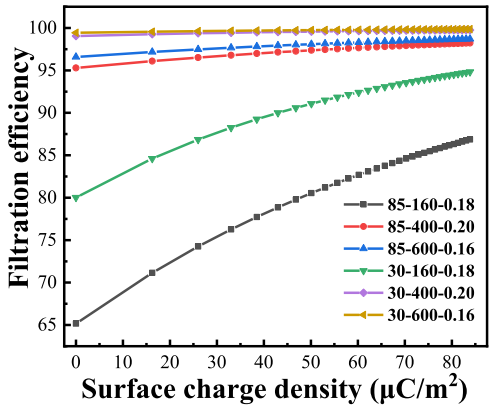

Figure 3. Filtration efficiency of the melt-blown layer as a function of the imposed surface charge density of fibers. The number of the first column in the legend indicates the flux, the second column indicates the thickness, and the third column indicates the fill rate. The diameter of filtering particles is 100 nm. Here, three typical melt-blown layers are selected.

gas fluxes of 30 L/min and 85 L/min, respectively. When the fiber diameter decreases, the filtration efficiency increases rapidly at the same fill rate. In the data of thickness 400 μm, it was found that reducing the fiber diameter from 3 to 2 μm can reduce the fiber fill rate from 0.16 to 0.1 and keep the efficiency above 90% at 85 L/min, which means that the areal density of the melt-blown layer can be reduced from 57.6 to 36 g/m^2. Similarly, if it is necessary to achieve a filtration efficiency of more than 95%, then the diameter of the fiber in the 400 μm thick melt-blown layer can be reduced from 3 μm to 2 μm, and the fill rate can be reduced from 0.2 to 0.12 (areal density from 72 to 43.2 g/m^2). From the point of view of filtration pressure drop, the above two cases can, respectively, reduce the pressure drop from 158 to 151 Pa and from 261 to 207 Pa, which means that reducing the fiber diameter while reducing the fill rate can reduce the pressure drop as much as possible under the same filtration efficiency. It is not difficult to find from Figures 4 and 5 that reducing the fiber diameter could be an effective method to reduce the cost while ensuring the quality of the melt-blown cloth.

Particles with different sizes for filtration are also an important factor in evaluating the performance of the melt-blown layer. In the data of Figure 6, there are two empirical parameters, A and m, in the calculation of the capture efficiency because of diffusion (E_D) related to the particle size. We performed an error evaluation based on the work of Wang et al.,[12] and detailed values of A and m are given in the Theory and Model section. The filtration efficiency of both melt-blown layers showed a trend of decrease first and then increased with the increase of particle diameter. The mechanical efficiency reaches the lowest value around the particle diameter of 0.2 μm, while the charged melt-blown layer has the worst filtering effect on particles of around 0.1 μm. This is mainly because of the fact that in Figure 6c,d, as the particle diameter increases, E_D decreases continuously and E_I and E_R increase. In other words, with the increase of particle size, the proportion of filtration efficiency caused by diffusion becomes smaller and smaller, and the proportion of capture efficiency caused by collision interception and inertia becomes larger and larger. Comparing the changes in the capture efficiency at the gas fluxes of 30 and 85 L/min, it was found that the increase in E_I at high gas velocity is faster than that at low gas velocity, which

https://dx.doi.org/10.1021/acs.iecr.0c06232
Ind. Eng. Chem. Res. 2021, 60, 1962−1971

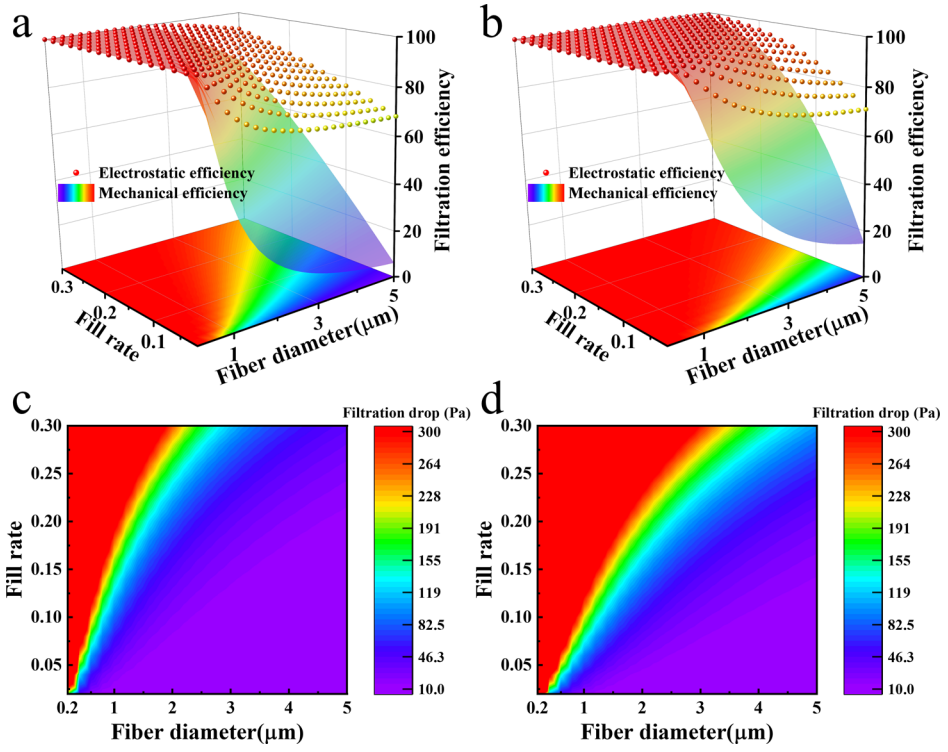

Figure 4. Filtration performances of melt-blown layers with different fiber diameters and fiber fill rates at 30 L/min. The preconditions of the data above are: thicknesses, 160 μm (a,c) and 400 μm (b,d); imposed surface charge density of fibers, 67 $\mu C/m^2$; filtering particles' diameter, 100 nm.

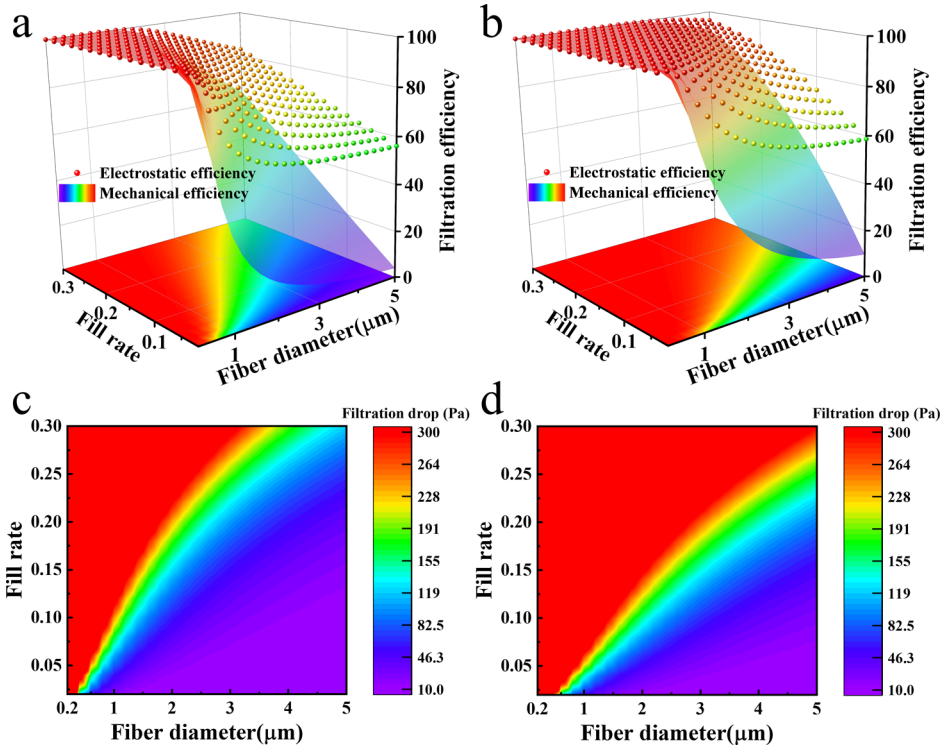

Figure 5. Filtration performances of melt-blown layers with different fiber diameters and fiber fill rates at 85 L/min. The preconditions of the data above are: thicknesses, 160 μm (a,c) and 400 μm (b,d); imposed surface charge density of fibers, 67 $\mu C/m^2$; filtering particles' diameter, 100 nm.

is consistent with the intuition that particles are more susceptible to flow field inertia under high-velocity gas flow. Also, we find that for melt-blown layers of different thicknesses, the trend of capture efficiency with particle diameter is basically the same, so here only 160 and 400 μm are taken as examples. Besides, the particle size at the lowest point of filtration efficiency will increase slightly as the thickness of the melt-blown layer increases.

Furthermore, the influence of the hydrophilicity of the fibers on the filtration performance is taken into consideration by

https://dx.doi.org/10.1021/acs.iecr.0c06232
Ind. Eng. Chem. Res. 2021, 60, 1962−1971

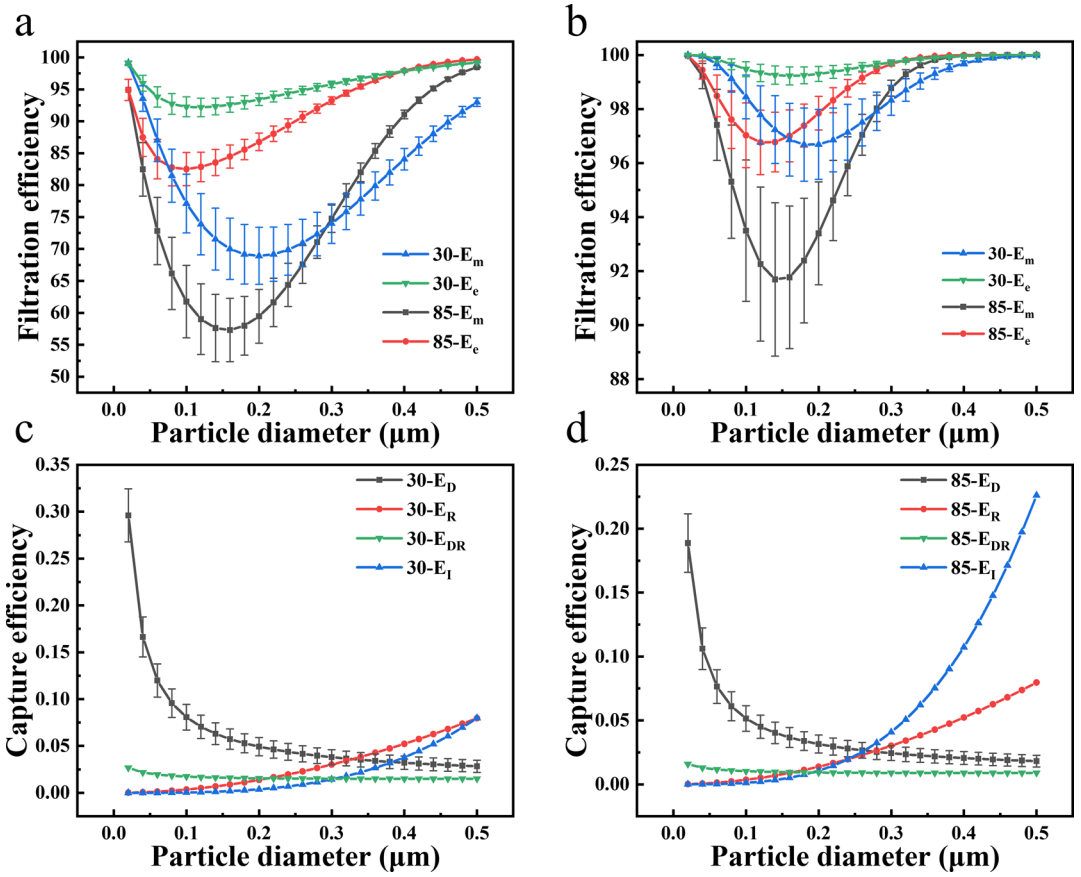

Figure 6. Filtration efficiency of the melt-blown layer (a,b) and capture efficiency of single fiber (c,d) as a function of particle diameter. The preconditions of the data are: thicknesses, 160 μm (a) and 400 μm (b,c,d); fill rate, 0.18 (a) and 0.2 (b,c,d); surface charge density of fibers, 67 $\mu C/m^2$.

MD simulations. From the snapshots in Figure 7, the contact angles of water droplets are 134° (hydrophobic), 91° (neutral), and 0° (completely hydrophilic) on the fixed slab, respectively. Then, the water droplets are pulled up in the Z direction at a speed of 5 Å/ns over time. Comparing the three surfaces, it can be found that the droplet becomes more and more difficult to separate from the surface until the liquid breaks up and a small droplet is separated under the condition of full spreading as the hydrophilicity increases (the contact angle decreases). Figure 7d shows the process of separating droplets on five different affinity surfaces. By integrating the force required to separate droplets, the potential of mean force was used to describe the difficulty of separation. The hydrophilic surface is more likely to adsorb water droplets than the hydrophobic surface, preventing the desorption. Therefore, a similar conclusion could be drawn that the oily droplets on lipophilic surfaces are more difficult to desorb. In the melt-blown layer, once the droplets are easily desorbed from the fiber surface, the filtration efficiency will be reduced.

In addition to desorption performance of droplets on the surface of hydrophilic and hydrophobic fibers, the water blocking properties of nanopores among the melt-blown fiber networks are studied by MD simulations. The nanopores are modeled by a (40,40) SWCNT vertically embedded between two layers of graphene, as Figure 8a shows. It can be found from the snapshots in Figure 8b that the nanopores with diameter ~54.24 Å in the hydrophobic fiber network exhibit excellent water blocking performance. In this simulation, the application of a pressure difference of 20 MPa still cannot make water flow through the pores with diameters of ~5.4 nm, which means that the hydrophobic melt-blown fibers have better ability to intercept aqueous particles containing viruses. On the contrary, the hydrophobic pore in Figure 8c can transport water without differential pressure.

To further demonstrate the theoretical analysis, the water contact angles and water blocking properties of two kinds of fibers were tested. Hydrophobic films of typical polypropylene melt-blown fibers obtained from commercially available masks were described as group #1. By soaking the films in cetrimonium bromide (CTAB) solution followed by drying treatment, the films exhibited significant hydrophilic properties, and the samples were described as group #2. As the results show in Figure 9a, the typical polypropylene melt-blown fibers show a water contact angle of ~138°. For the sample in group #2, the contact angles changed from 94.2° to 54° within 5 min and the water droplets are easily absorbed by the hydrophilic films. As the experiments in Figure 9b illustrate, the typical polypropylene melt-blown fibers exhibit excellent water blocking performance, while the melt-blown fibers treated by hydrophilic surfactants are easily penetrated by water. Comparing the weights of two kinds of melt-blown fibers before and after water penetration (in Figure 9b), it can be found that the melt-blown fibers treated by CTAB obviously have a stronger ability to absorb water. The experimental results illustrate that the surface affinity has a great influence on the performance of the melt-blown fibers. Generally, hydrophilic fibers can adhere to viruses and the hydrophobic network can block water-based particles in the airflow. A

https://dx.doi.org/10.1021/acs.iecr.0c06232
Ind. Eng. Chem. Res. 2021, 60, 1962−1971

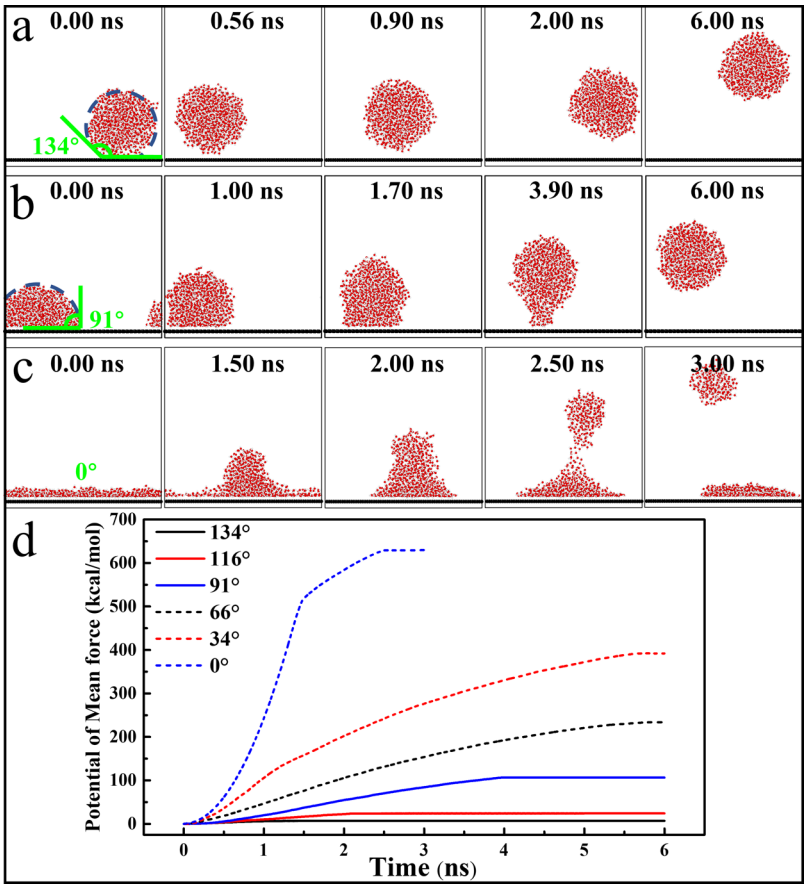

Figure 7. Snapshots of the desorption process of water droplets on different affinity surfaces (a–c) and the curves of the potential of mean force of the desorption process (d). The black balls (C atoms) in the bottom lines in (a–c) are the side views of the graphene slabs, and the red and white balls (O and H atoms) form water droplets.

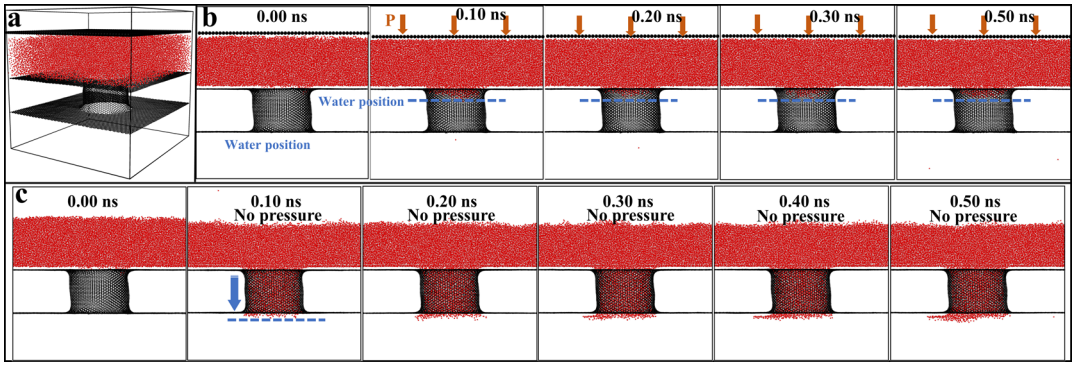

Figure 8. Model for simulating water blocking properties of pores in melt-blown fiber network (a). Snapshots of water entering the hydrophobic pore by applying a pressure of 20 MPa above the pore (b). Snapshots of water entering the hydrophilic pore without differential pressure between the two sides of the pore (c).

hydrophilic–hydrophobic–hydrophilic sandwich structure of the melt-blown intermediate layer would be beneficial for maintaining the protective performance of the respirator.

Finally, the smaller the fiber diameter is, the easier it is to improve the performance of melt-blown cloth, which is discussed in more depth. Using SWCNT as a model, the snapshots of water droplets with different speeds impacting two fixed nanofibers of different diameters were revealed by MD simulations. The force field parameters of fibers are consistent with the surface with a contact angle of 134° based on the results in Figure 7. According to the simulation results shown in Figure 10, when the water droplet speed reaches 7 Å/ps, it can be broken by the nanofiber with a diameter of 6.78 Å. However, a minimum speed of 9 Å/ps is needed for droplets to be cut by the nanofiber with a diameter of 27.12 Å. Because of the limitation of calculation ability, it is hard to directly simulate the micron and submicron systems. It is not difficult to conclude that it is easier for fibers with smaller diameters to break particulates (especially large particulates) into small particulates. Although reducing the fiber diameter can improve filtration efficiency while achieving small air resistance (as Figure 5 shows), the effects of fibers on the coalescence and

https://dx.doi.org/10.1021/acs.iecr.0c06232
Ind. Eng. Chem. Res. 2021, 60, 1962–1971

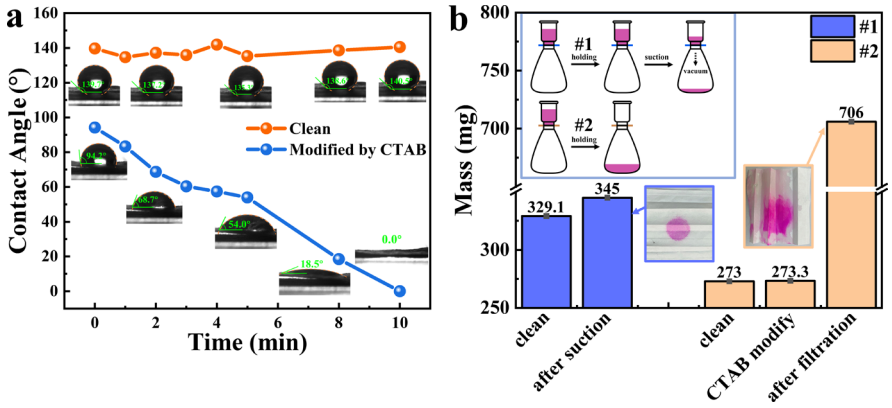

Figure 9. Water droplet contact angles and snapshots of the clean melt-blown cloth and the melt-blown cloth modified by CTAB (a). Schematic of water blocking experiments using these two types of melt-blown cloth and the mass changes of two types of melt-blown cloth after penetration by water (b). In figure (b), rhodamine B is added to deionized water to enhance the display, and the illustration shows the corresponding experimental operation process.

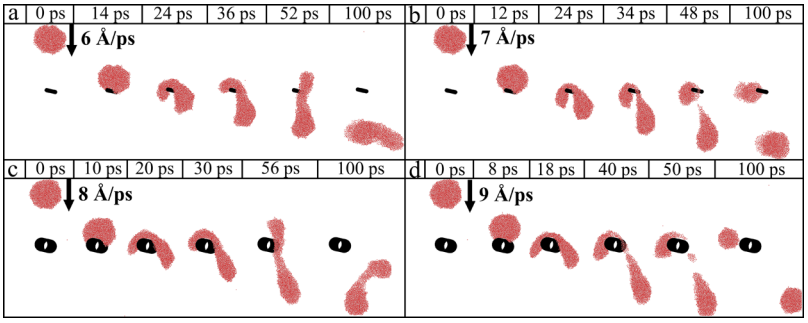

Figure 10. Snapshots of coalescence and fragmentation of water droplets with different speeds impacted by fibers with diameters at a nanoscale. The diameters of fibers are (a,b) 6.78 Å and (c,d) 27.12 Å, respectively. The black cylinders represent the fibers.

fragmentation of particulates should also be taken into account when designing melt-blown fibers for the filtering layer of a mask.

4. CONCLUSIONS

In conclusion, we present a systematic study on the complexity of respirator design through cross-scale simulations by optimizing the models of filter media for the middle layer filtration process. As the thickness and fill rate of the melt-blown layer increase, the filtration efficiency increases, while the filtration pressure drop also increases. Moreover, when the thickness (<200 μm) and fill rate (<20%) are small, increasing them has a remarkable effect on the filtration efficiency. As the surface electrostatic potential increases (>65 $\mu C/m^2$), the improvement of filtration efficiency is tiny. The filtration efficiencies of layers with different fill rates and different fiber diameters were also investigated. It was found that reducing the fiber diameter can reduce the areal density of the melt-blown layer, which is beneficial for improving filtration, thus to reduce the usage of polypropylene materials. As the particle diameter increases, the filtration efficiency tends to decrease first and then increase, and generally has the worst filtration effect on particles with a diameter of 0.1−0.2 μm. MD simulations were also involved to study the droplet adhesion and water blocking performance of different affinity melt-blown fibers. For the adsorption of different particulates (aqueous, oily, etc.), the affinity of materials should be considered to make the melt-blown layer achieve a good performance. When designing melt-blown fibers for the filtering layer of a mask, a hydrophilic−hydrophobic−hydrophilic sandwich structural middle layer should be beneficial for maintaining the protective performance of the respirator for the prevention of water-based particles. The effects of fibers on the coalescence and fragmentation of particulates should also be taken into account. Current standards related to respirators mainly focus on the initial performance of the products. Despite the fact that some industry associations are paying attention to release standards to ensure the quality and life of masks for multiple reuses, conventional studies less-related the reliability design of respirators under complicated working conditions. We hope the findings in our work can stimulate new ideas and inspire new products of respirators with improving protection against the pandemic.

AUTHOR INFORMATION

Corresponding Authors

Bao-Chang Sun − *State Key Laboratory of Organic Inorganic Composites, Beijing University of Chemical Technology, Beijing 100029, China; Research Center of the Ministry of Education for High Gravity Engineering and Technology, Beijing University of Chemical Technology, Beijing 100029, China;* orcid.org/0000-0002-3435-1250; Email: sunbc@mail.buct.edu.cn

Dan Wang − *State Key Laboratory of Organic Inorganic Composites, Beijing University of Chemical Technology, Beijing 100029, China; Research Center of the Ministry of Education for High Gravity Engineering and Technology, Beijing University of Chemical Technology, Beijing 100029,*

https://dx.doi.org/10.1021/acs.iecr.0c06232
Ind. Eng. Chem. Res. 2021, 60, 1962−1971

China; orcid.org/0000-0002-3515-4590; Email: wangdan@mail.buct.edu.cn

Authors

Jie Shi − *State Key Laboratory of Organic Inorganic Composites, Beijing University of Chemical Technology, Beijing 100029, China; Research Center of the Ministry of Education for High Gravity Engineering and Technology, Beijing University of Chemical Technology, Beijing 100029, China*

Yuanzuo Zou − *State Key Laboratory of Organic Inorganic Composites, Beijing University of Chemical Technology, Beijing 100029, China; Research Center of the Ministry of Education for High Gravity Engineering and Technology, Beijing University of Chemical Technology, Beijing 100029, China*

Jie-Xin Wang − *State Key Laboratory of Organic Inorganic Composites, Beijing University of Chemical Technology, Beijing 100029, China; Research Center of the Ministry of Education for High Gravity Engineering and Technology, Beijing University of Chemical Technology, Beijing 100029, China;* orcid.org/0000-0003-0459-1621

Xiao-Fei Zeng − *State Key Laboratory of Organic Inorganic Composites, Beijing University of Chemical Technology, Beijing 100029, China; Research Center of the Ministry of Education for High Gravity Engineering and Technology, Beijing University of Chemical Technology, Beijing 100029, China;* orcid.org/0000-0001-9010-0088

Guang-Wen Chu − *State Key Laboratory of Organic Inorganic Composites, Beijing University of Chemical Technology, Beijing 100029, China; Research Center of the Ministry of Education for High Gravity Engineering and Technology, Beijing University of Chemical Technology, Beijing 100029, China;* orcid.org/0000-0002-3047-7024

Jian-Feng Chen − *State Key Laboratory of Organic Inorganic Composites, Beijing University of Chemical Technology, Beijing 100029, China; Research Center of the Ministry of Education for High Gravity Engineering and Technology, Beijing University of Chemical Technology, Beijing 100029, China*

Complete contact information is available at: https://pubs.acs.org/10.1021/acs.iecr.0c06232

Author Contributions

The manuscript was written through contributions of all authors. All authors have given approval to the final version of the manuscript.

Notes

The authors declare no competing financial interest.

■ ACKNOWLEDGMENTS

We are grateful for financial support from the National Key Research and Development Program of China (2020YFC0844800) and National Natural Science Foundation of China (91934303). This work was supported by the High Performance Computing Platform of BUCT.

■ REFERENCES

(1) Leung, N. H. L.; Chu, D. K. W.; Shiu, E. Y. C.; Chan, K.-H.; McDevitt, J. J.; Hau, B. J. P.; Yen, H.-L.; Li, Y.; Ip, D. K. M.; Peiris, J. S. M.; Seto, W.-H.; Leung, G. M.; Milton, D. K.; Cowling, B. J. Respiratory virus shedding in exhaled breath and efficacy of face masks. *Nat. Med.* **2020**, *26*, 676−680.

(2) Mackenzie, D. Reuse of N95 masks. *Engineering* **2020**, *6*, 593−596.

(3) Wang, D.; Sun, B.-C.; Wang, J.-X.; Zhou, Y.-Y.; Chen, Z.-W.; Fang, Y.; Yue, W.-H.; Liu, S.-M.; Liu, K.-Y.; Zeng, X.-F.; Chu, G.-W.; Chen, J.-F. Can masks be reused after hot water decontamination during the COVID-19 pandemic? *Engineering* **2020**, *6*, 1115−1121.

(4) Konda, A.; Prakash, A.; Moss, G. A.; Schmoldt, M.; Grant, G. D.; Guha, S. Aerosol filtration efficiency of common fabrics used in masky cloth masks. *ACS Nano* **2020**, *14*, 6339−6347.

(5) Drabek, J.; Zatloukal, M. Meltblown technology for production of polymeric microfibers/nanofibers: A review. *Phys. Fluids* **2019**, *31*, 091301.

(6) Jung, H.; Kim, J. K.; Lee, S.; Lee, J.; Kim, J.; Tsai, P.; Yoon, C. Comparison of filtration efficiency and pressure drop in anti-yellow sand masks, quarantine masks, medical masks, general masks, and handkerchiefs. *Aerosol Air Qual. Res.* **2014**, *14*, 991−1002.

(7) Wang, J.; Kim, S. C.; Pui, D. Y. H. Carbon nanotube penetration through a screen filter: Numerical modeling and comparison with experiments. *Aerosol Sci. Technol.* **2011**, *45*, 443−452.

(8) Kim, S. H.; Lee, K. W. Experimental study of electrostatic precipitator performance and comparison with existing theoretical prediction models. *J. Electrost.* **1999**, *48*, 3−25.

(9) Ghatak, B.; Banerjee, S.; Ali, S. B.; Bandyopadhyay, R.; Das, N.; Mandal, D.; Tudu, B. Design of a self-powered triboelectric face mask. *Nano Energy* **2021**, *79*, 105387.

(10) Hossain, E.; Bhadra, S.; Jain, H.; Das, S.; Bhattacharya, A.; Ghosh, S.; Levine, D. Recharging and rejuvenation of decontaminated N95 masks. *Phys. Fluids* **2020**, *32*, 093304.

(11) Liao, L.; Xiao, W.; Zhao, M.; Yu, X.; Wang, H.; Wang, Q.; Chu, S.; Cui, Y. Can N95 masks be reused after disinfection? How many times? *ACS Nano* **2020**, *14*, 6348−6356.

(12) Wang, J.; Chen, D. R.; Pui, D. Y. H. Modeling of filtration efficiency of nanoparticles in standard filter media. *J. Nanopart. Res.* **2006**, *9*, 109−115.

(13) Wang, J.; Pui, D. Y. H. Filtration of aerosol particles by elliptical fibers: a numerical study. *J. Nanopart. Res.* **2009**, *11*, 185−196.

(14) Lee, K. W.; Liu, B. Y. H. On the minimum efficiency and the most penetrating particle size for fibrous filters. *J. Air Pollut. Control Assoc.* **1980**, *30*, 377−381.

(15) Wang, J.; Kim, S. C.; Pui, D. Y. H. Measurement of multi-wall carbon nanotube penetration through a screen filter and single-fiber analysis. *J. Nanopart. Res.* **2011**, *13*, 4565−4573.

(16) Bénesse, M.; Coq, L. L.; Solliec, C. Collection efficiency of a woven filter made of multifiber yarn: Experimental characterization during loading and clean filter modeling based on a two-tier single fiber approach. *J. Aerosol Sci.* **2006**, *37*, 974−989.

(17) Hinds, W. C. *Aerosol Technology: Properties, Behavior, and Measurement of Airborne Particles*; John Wiley & Sons: New York, 2012.

(18) Stechkina, I. B.; Fuchs, N. A. Studies on fibrous aerosol filters—I. Calculation of diffusional deposition of aerosols in fibrous filters. *Ann. Occup. Hyg.* **1966**, *9*, 59−64.

(19) Kuwabara, S. The forces experienced by randomly distributed parallel circular cylinders or spheres in a viscous flow at small reynolds numbers. *J. Phys. Soc. Jpn.* **1959**, *14*, 527−532.

(20) Liu, Z. G.; Wang, P. K. Pressure drop and interception efficiency of multifiber filters. *Aerosol Sci. Technol.* **1997**, *26*, 313−325.

(21) Yu, T.; Zhao, Y.-b. Computational modeling of filtration efficiency of electret air filter media. *J. Filtr. Sep.* **2017**, *27*, 27−32.

(22) Chang, D.-Q.; Chen, S.-C.; Fox, A. R.; Viner, A. S.; Pui, D. Y. H. Penetration of sub-50 nm nanoparticles through electret HVAC filters used in residence. *Aerosol Sci. Technol.* **2015**, *49*, 966−976.

(23) Plimpton, S. Fast parallel algorithms for short-range molecular dynamics. *J. Comput. Phys.* **1995**, *117*, 1−19.

(24) Lennard-Jones, J. E. Cohesion. *Proc. Phys. Soc.* **1931**, *43*, 461−482.

(25) Li, J.; Wang, F. Water graphene contact surface investigated by pairwise potentials from force-matching PAW-PBE with dispersion correction. *J. Chem. Phys.* **2017**, *146*, 054702.